Simona Perotto

Anisotropic mesh adaption: application to computational fluid dynamics

<$<$http://www.bdim.eu/item?id=BUMI_2005_8_8B_1_145_0$>$

Anisotropic Mesh Adaption: Application
to Computational Fluid Dynamics.

Simona Perotto (*)

Sunto. – *In questa comunicazione vengono presentate tecniche di adattazione di griglia goal-oriented di tipo anisotropo. Punto di partenza è stata la derivazione di opportune stime di tipo anisotropo per l'errore d'interpolazione, per elementi finiti lineari a pezzi, su griglie triangolari in 2D. Si sono quindi utilizzate tali stime d'interpolazione per generalizzare al caso anisotropo l'analisi a posteriori proposta da R. Rannacher e da R. Becker, basata su un approccio di tipo duale. In questo lavoro tale analisi a posteriori viene particolarizzata al caso di problemi ellittici, di trasporto-diffusione-reazione e al problema di Stokes. Vengono da ultimo forniti alcuni risultati numerici al fine di validare l'affidabilità dell'approccio proposto.*

Summary. – *In this communication we focus on goal-oriented anisotropic adaption techniques. Starting point has been the derivation of suitable anisotropic interpolation error estimates for piecewise linear finite elements, on triangular grids in 2D. Then we have merged these interpolation estimates with the dual-based a posteriori error analysis proposed by R. Rannacher and R. Becker. As examples of this general anisotropic a posteriori analysis, elliptic, advection-diffusion-reaction and the Stokes problems are analyzed. Finally, numerical test cases are provided to assess the soundness of the proposed approach.*

1. – Motivations.

In Computational Fluid Dynamics (CFD), as well as in many other engineering areas, mesh adaption is widely used. The leading idea is to reduce the computational cost associated with the approximation of the phenomenon at hand by distributing the mesh triangles according to the solution behaviour. We mainly distinguish between heuristic and theoretically based adaption techniques. In the first case geometric information, such as estimates of the gradient or of the Hessian of the numerical solution, are essentially exploited. For instance, this is the case of the well-known Zienkiewicz-Zhu error estimator [39, 40, 41]. On the other hand, more theoretically sound approaches move from suitable a priori and a posteriori estimates of the discretization error. In this framework the reference literature is extensive (see, e.g., [1, 5, 6, 7, 16, 25, 34, 38].

(*) Comunicazione presentata a Milano in occasione del XVII Congresso U.M.I.

In the beginning, both heuristic and theoretical strategies have been used essentially to deal with isotropic computational grids. More recently, the interest has moved towards anisotropic mesh adaption as more efficient in tackling problems characterized by directional features, that is great variations along certain directions with less significant changes along other ones (e.g., shocks, boundary and internal layers, singularities). An example of anisotropic behaviour is provided by the function $w(x_1, x_2) = [-0.5 \log((x_1 - 0.5)^2 + (x_2 - 0.5)^2)]^{1/4}$ in Fig. 1, the computational domain Ω being the disk of radius $r = 0.6$, centered at $(0.5, 0.5)$. The function $w \in H^1(\Omega) \setminus H^2(\Omega)$ is affected by an internal singularity at $(0.5, 0.5)$.

The leading idea of an anisotropic approach reads as follows: reduce the number of degrees of freedom involved in the approximation of the problem at hand for a fixed solution accuracy, or vice versa, given a constraint on the number of elements, find the mesh maximizing the accuracy of the numerical solution, by better orienting the mesh elements according to some suitable features of the solution.

For the function w above, we have chosen, according to the second approach, to compare an isotropic with an anisotropic mesh both approximatively of 5700 elements (see Fig. 1, bottom line). By comparing the L^2-norms of the
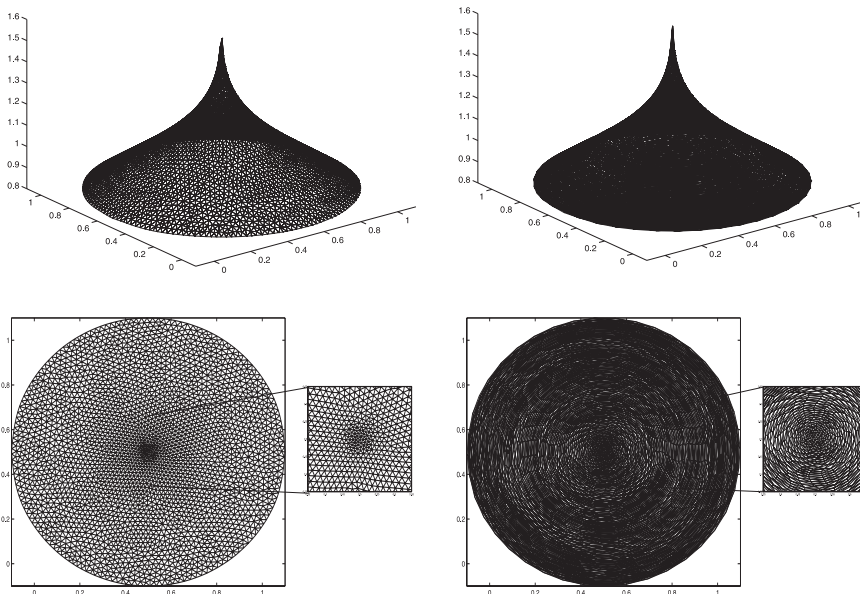
Fig. 1. – Plots (top line) of the function w on an isotropic mesh (bottom-left) and on an anisotropic one (bottom-right) driven by an L^2-error a priori estimator.

discretization error $\|e_h\|$, we get $\|e_h\|^{\text{iso}} = 9.7\,e - 04$ and $\|e_h\|^{\text{aniso}} = 3.6\,e - 04$, i.e., a reduction of nearly one-third on the anisotropic grid. The gain is greater (even one order!) if we consider the mean-value of the L^2-norms with respect to the number of elements, as $(\text{mean}\,\|e_h\|^{\text{iso}}) = 1.2\,e - 05$ and $(\text{mean}\,\|e_h\|^{\text{aniso}}) = 1.2\,e - 06$. Moreover, it is evident that in the anisotropic case the mesh is characterized by concentric zones of stretched triangles: as expected, the triangles align their longest edges perpendicularly to the direction of maximal variation, i.e., the radial one.

The results above show an improvement in the approximation quality on the anisotropic grid with respect to the isotropic case. However, the main drawback characterizing an anisotropic approach is the higher computational cost justified by the more complex analysis required to fully describe the element dimensions and orientation. Thus, it turns out to be convenient an anisotropic approach instead of the more traditional isotropic one when the decrease of the computational cost due to the reduction of the degrees of freedom exceeds the increase of the computational complexity associated with the anisotropic description of the mesh triangles.

Anisotropic analyses of different type are available in the most recent literature (see, e.g., [3, 12, 13, 23, 26, 30, 35, 37]). Concerning our approach, we have moved from the derivation of anisotropic interpolation error estimates for piecewise linear finite elements. This has been obtained by exploiting the spectral properties of the standard affine mapping between the reference and the general mesh element [17]. Then we have merged these estimates with the dual-based a posteriori error analysis proposed by R. Rannacher and R. Becker [18]. This approach turns out to be suitable for a goal-oriented adaptivity as it allows us to control energy norms as well as suitable functionals of the discretization error.

The outline of the paper is the following. In Sect. 2, after introducing some notations for the functional environment, we provide the anisotropic framework for finite elements. Sect. 3 is devoted to the anisotropic interpolation error estimates. These represent the main tool used in the a posteriori error analysis addressed in Sect. 4. First, this analysis is discussed in the case of a general linear differential operator and then it is detailed for the elliptic, the advection-diffusion-reaction and the Stokes problems. Finally, in Sect. 5 the effectiveness of the proposed anisotropic analysis is assessed on some numerical test cases.

2. – Abstract frameworks.

2.1. *Functional setting*.

In what follows a standard notation is adopted for the Sobolev spaces of functions with Lebesgue-measurable derivatives, and for their norms [31]. Let

$W^{k,p}(\Omega) = \{v \in L^p(\Omega): D^{\boldsymbol{\alpha}}v \in L^p(\Omega), \forall \boldsymbol{\alpha} \text{ s.t. } |\boldsymbol{\alpha}| \leq k\}$ be the Sobolev space of functions for which the p-th power of their distributional derivatives of order up to $k \geq 0$ is Lebesgue-measurable, with $1 \leq p < \infty$, $\Omega \subset \mathbb{R}^d$ and $d = 1, 2, 3$. In particular, for $p = 2$, we let $W^{k,2}(\Omega) = H^k(\Omega)$ and when $k = 0$, we have the space $L^2(\Omega)$ of square-integrable functions. Moreover, $H_0^1(\Omega)$ denotes the space of H^1-functions identically equal to zero on the boundary $\partial\Omega$ of the domain, while $H_{\Gamma_D}^1(\Omega)$ stands for the set of H^1-functions equal to zero only on the portion Γ_D of the boundary domain. We also recall that $L^\infty(\Omega)$ is the space of bounded functions a.e., while $W^{1,\infty}(\Omega) \subset L^\infty(\Omega)$ is such that also the first derivatives are bounded a.e. Finally, $C^0(\overline{\Omega})$ denotes the space of continuous functions on $\overline{\Omega}$.

The norms and seminorms defined on a generic functional space V will be denoted below with $\|\cdot\|_V$ and $|\cdot|_V$, respectively.

2.2. *An anisotropic setting for finite elements.*

Let $\Omega \subset \mathbb{R}^2$ be a polygonal domain and, for any $0 < h \leq 1$, let $\{\mathcal{C}_h\}_h$ be a family of conforming triangulations of $\overline{\Omega}$ into triangles K of diameter $h_K \leq h$.

Following the idea proposed in [17], the additional information for the geometrical description of the mesh elements is derived from the standard affine transformation $T_K: \widehat{K} \to K$, with $K = M_K(\widehat{K}) + \boldsymbol{b}_K$, $M_K \in \mathbb{R}^{2 \times 2}$ and $\boldsymbol{b}_K \in \mathbb{R}^2$, from the reference triangle $\widehat{K}$ into K, where $\widehat{K}$ can be, e.g., the right triangle $(0,0)$, $(1,0)$, $(0,1)$ or the equilateral one $(-1/2, 0)$, $(1/2, 0)$, $(0, \sqrt{3}/2)$ (see Fig. 2). Let $M_K = B_K Z_K$ be the polar decomposition of the invertible matrix M_K, with B_K and Z_K a symmetric positive definite and an orthogonal matrix, respectively. Then the matrix B_K is factorized in terms of its eigenvalues $\lambda_{i,K}$ (with $\lambda_{1,K} \geq \lambda_{2,K}$) and eigenvectors $\boldsymbol{r}_{i,K}$, for $i = 1, 2$, as $B_K = R_K^T \Lambda_K R_K$, where $\Lambda_K = \text{diag}(\lambda_{1,K}, \lambda_{2,K})$ and $R_K = [\boldsymbol{r}_{1,K}, \boldsymbol{r}_{2,K}]^T$. As shown in Fig. 2, the eigenvectors $\boldsymbol{r}_{i,K}$ provide the directions of the semi-axes of the ellipse circum-
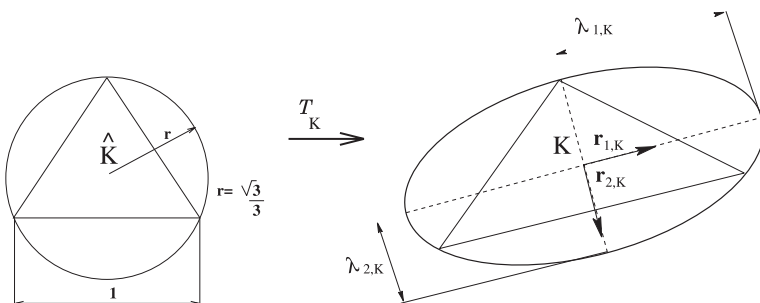
Fig. 2. – The standard affine transformation T_K from the reference triangle $\widehat{K}$ into the general one K.

scribed to the element K, while the eigenvalues $\lambda_{i,K}$ measure the length of such semi-axes. It turns out that the shape and orientation of each triangle K are identified by the quantities $\boldsymbol{r}_{i,K}$ and $\lambda_{i,K}$. Finally, the deformation of K with respect to the generic element $\widehat{K}$ is measured by the so-called *stretching factor* $s_K = \lambda_{1,K}/\lambda_{2,K}(\geqslant 1)$, being $s_{\widehat{K}} = 1$.

3. – Anisotropic interpolation error estimates.

First step towards the anisotropic a posteriori analysis provided in Sect. 4 has been the derivation of suitable interpolation error estimates [17, 18, 32].

We have derived anisotropic estimates for both the Lagrange and the Clément-like interpolants [10, 11] due to the different regularity characterizing the function to be interpolated. Denoting by W_h the finite element space of continuous affine functions, let $\Pi_h: C^0(\overline{\Omega}) \to W_h$ and $I_h: L^2(\Omega) \to W_h$ be the Lagrange and Clément linear interpolants, respectively and let their restrictions to each element $K \in \mathcal{C}_h$ be Π_K and I_K. We can state the results below.

PROPOSITION 3.1. – *Let $v \in H^2(K)$, for any $K \in \mathcal{C}_h$. Then there exist two constants $C_1 = C_1(\widehat{K})$ and $C_2 = C_2(\widehat{K})$ such that*

$$(1) \qquad \|v - \Pi_K(v)\|_{L^2(K)} \leqslant C_1 \left[\sum_{i,j=1}^{2} \lambda_{i,K}^2 \lambda_{j,K}^2 L_K^{ij}(v) \right]^{1/2},$$

$$|v - \Pi_K(v)|_{H^1(K)} \leqslant C_2 \lambda_{2,K}^{-1} \left[\sum_{i,j=1}^{2} \lambda_{i,K}^2 \lambda_{j,K}^2 L_K^{ij}(v) \right]^{1/2},$$

where

$$(2) \qquad L_K^{ij}(v) = \int_K (\boldsymbol{r}_{i,K}^T H_K(v)\, \boldsymbol{r}_{j,K})^2\, d\boldsymbol{x}, \quad with \ \ i,j = 1, 2,$$

$H_K(v)$ *is the Hessian matrix associated with $v|_K$, and $\boldsymbol{x} = (x_1, x_2)^T \in K$.*

PROPOSITION 3.2. – *Let $v \in H^1(\Omega)$. Then there exist two constants $C_3 = C_3(M, \widehat{C})$ and $C_4 = C_4(M, \widehat{C})$ such that, for any $K \in \mathcal{C}_h$,*

$$(3) \qquad \|v - I_K(v)\|_{L^2(K)} \leqslant C_3 \left[\sum_{i=1}^{2} \lambda_{i,K}^2 (\boldsymbol{r}_{i,K}^T G_K(v)\, \boldsymbol{r}_{i,K}) \right]^{1/2},$$

$$|v - I_K(v)|_{H^1(K)} \leqslant C_4 \lambda_{2,K}^{-1} \left[\sum_{i=1}^{2} \lambda_{i,K}^2 (\boldsymbol{r}_{i,K}^T G_K(v)\, \boldsymbol{r}_{i,K}) \right]^{1/2},$$

where $G_K(v) \in \mathbb{R}^{2 \times 2}$ is the symmetric positive semi-definite matrix with entries $(G_K(v))_{i,j} = \int_{\Delta_K} \partial v / \partial x_i\, \partial v / \partial x_j\, d\boldsymbol{x}$, Δ_K is the patch of all the elements shar-

ing a vertex with K, and $M \in \mathbb{N}$ and $\widehat{C} > 0$ are the constants defined through the relations

(4) $$\operatorname{card}(\Delta_K) \leqslant M \quad and \quad \operatorname{diam}(\Delta_{\widehat{K}}) \leqslant \widehat{C},$$

with $\Delta_{\widehat{K}} = T_K^{-1}(\Delta_K)$.

REMARK 3.1. – *Requirements* (4) *demand the cardinality of any patch* Δ_K *as well as the diameter of the reference patch* $\Delta_{\widehat{K}}$ *to be uniformly bounded independently of the geometry of the mesh. In particular, the latter inequality rules out some too distorted reference patches (see Fig. 2.1 in* [32]). *Moreover, notice that the definition provided in Proposition 3.2 for the patch* Δ_K *holds if* I_h *is the Clèment interpolant. It can be suitably modified when another Clèment-like interpolant is considered* [36].

The anisotropic estimates in Propositions 3.1 and 3.2 are certainly more complex than the corresponding isotropic ones. For instance, let us consider the isotropic results corresponding to (1) and (3), given by

(5) $$\|v - \Pi_K(v)\|_{L^2(K)} \leqslant C_1^* h_K^2 |v|_{H^2(K)} \text{ and } \|v - I_K(v)\|_{L^2(K)} \leqslant C_3^* h_K |v|_{H^1(\Delta_K)},$$

respectively, with $C_1^* = C_1^*(\widehat{K})$ and C_3^* depends essentially on the regularity of the mesh. From a dimensional viewpoint, we have both in (1) and in (5)$_1$ the square of the spacing parameters (i.e., h_K in the isotropic case, $\lambda_{1,K}$, $\lambda_{2,K}$ in the anisotropic one) as well as in (3) and (5)$_2$ the spacing parameters are involved. On the other hand, the H^2- and the H^1-seminorm of v in (5) are replaced in (1) and (3) by suitable sums of the $L_K^{i,j}(v)$ and of the $(r_{i,K}^T G_K(v) r_{i,K})$ quantities. We claim that the information provided by the seminorms $|v|_{H^2(K)}$ and $|v|_{H^1(\Delta_K)}$ have been split along the directions $r_{1,K}$ and $r_{2,K}$ via the anisotropic quantities $L_K^{i,j}(v)$ and $(r_{i,K}^T G_K(v) r_{i,K})$, representing the squared L^2-norms of the directional second- and first-order derivatives of v, respectively. As anticipated in Sect. 1, we are replacing the «lumped» isotropic results with more «distributed» ones. The pay-off of such a framework is that we are able to finely tune the adapted meshes in terms of shape and orientation of the elements.

Finally, in view of the a posteriori analysis of Sect. 4, we also need anisotropic estimates for the L^2-norm of the interpolation error on the edges e of the triangulation $\mathcal{T}_h$, i.e.,

$$\|v - \Pi_K(v)\|_{L^2(e)} \leqslant C_5 \left(\frac{\lambda_{1,K}^2 + \lambda_{2,K}^2}{\lambda_{2,K}^3} \right)^{1/2} \left[\sum_{i,j=1}^{2} \lambda_{i,K}^2 \lambda_{j,K}^2 L_K^{i,j}(v) \right]^{1/2}$$

and

$$\|v - I_K(v)\|_{L^2(e)} \leqslant C_6 \ \frac{1}{\lambda_{2,K}^{1/2}} \left[\sum_{i=1}^{2} \lambda_{i,K}^2 \big(\boldsymbol{r}_{i,K}^T G_K(v) \, \boldsymbol{r}_{i,K} \big) \right]^{1/2},$$

with $C_5 = C_5(\widehat{K})$ and $C_6 = C_6(M, \widehat{C})$, respectively.

4. – Anisotropic a posteriori error analysis: the general procedure.

In this section we show how to control suitable linear continuous functionals $J(\cdot)$ of the discretization error e_h associated with a finite element approximation of the problem at hand. Our starting point has been the a posteriori dual-based approach developed in [7]. Examples of functionals $J(\cdot)$ in CFD are the lift and drag around bodies in external flows or mean and local values, while in structural mechanics the torsion moment, the pointwise stresses or the surface tension are typical goal quantities. The leading idea of our a posteriori analysis is to combine the advantages characterizing an error functional control with the richness of information provided by an anisotropic framework.

Let us sketch the general procedure to derive an anisotropic a posteriori error estimator for a differential linear problem of the form

$$(6) \qquad\qquad\qquad L(u) = f \quad \text{in } \Omega,$$

completed with suitable boundary conditions. In what follows such a procedure will be particularized to standard model problems in CFD. We refer to [18, 19, 20] for a detailed description.

Let us move from the weak form associated with (6): find $u \in V$ such that

$$(7) \qquad\qquad\qquad a(u, v) = F(v) \quad \text{for any} \quad v \in V,$$

where V is a suitable functional space accounting for the boundary conditions associated with (6), and $a(\cdot, \cdot)$ and $F(\cdot)$ are the bilinear and linear forms corresponding to the differential operator L and the source term f, respectively. The discrete formulation of (7) is obtained by projecting onto the space $V_h \subset V$ of continuous piecewise linear finite elements which yields: find $u_h \in V_h$ such that

$$(8) \qquad\qquad\qquad a(u_h, v_h) = F(v_h) \quad \text{for any} \quad v_h \in V_h.$$

As stated in Sects. 4.2 and 4.3, the forms $a(\cdot, \cdot)$ and $F(\cdot)$ have to be suitably stabilized to deal with strong advective/reactive terms, or with the Stokes problem to guarantee the absence of spurious oscillations or the well-posedness of the problem, respectively.

Thus, by suitably combining the weak form (with $v = v_h$) with the discrete one, we get

$$(9) \qquad\qquad a(e_h, v_h) = 0 \quad \text{for any} \quad v_h \in V_h,$$

i.e., the well-known Galerkin orthogonality property stating the orthogonality of the discretization error $e_h = u - u_h$ with respect to the discrete space V_h.

Let us introduce now the dual problem associated with (7): find $z \in V$ such that

$$(10) \qquad\qquad a^*(z, \varphi) = J(\varphi) \quad \text{for any} \quad \varphi \in V,$$

where J is a linear continuous functional chosen according to the physical quantity to control and $a^*(\cdot, \cdot)$ is the adjoint form to $a(\cdot, \cdot)$, defined by the relation $a^*(z, \varphi) = a(\varphi, z)$, for any $\varphi, z \in V$.

We are now in a position to estimate the discretization error associated with the goal quantity, that is $J(e_h)$. With this aim, let us first choose in (10) $\varphi = e_h$. Then by exploiting the property of the adjoint form $a^*(\cdot, \cdot)$ and the Galerkin orthogonality property (9), with $v_h = z_h$, we get

$$(11) \qquad J(e_h) = a^*(z, e_h) = a(e_h, z) = a(e_h, z - z_h) = F(z - z_h) - a(u_h, z - z_h),$$

where, in the last equality, the weak form (7), with $v = z - z_h$, has been used. So far we have not explicitly chosen z_h. Usually, z_h is identified with a suitable interpolant of the dual solution z, according to the regularity of this latter. An elementwise integration by parts of the right-hand side of (11) together with a suitable use of anisotropic interpolation error estimates such as those cited in Sect. 3, lead to an a posteriori error estimate of the general form

$$(12) \qquad\qquad |J(e_h)| \leq C \sum_{K \in \mathcal{C}_h} \varrho_K(u_h) \, \omega_K(z),$$

where $\varrho_K(u_h)$ is the elemental residual associated with the primal problem (6) taking into account internal and edge contributions, and $\omega_K(z)$, which gathers the anisotropic information, depends on the dual solution and weights the residual term. We remark that $\varrho_K(u_h)$ measures the error related to the approximation u_h, while the term $\omega_K(z)$ takes into account the propagation of such an error driven by the functional $J(\cdot)$ to control.

In Sects. 4.1, 4.2 and 4.3 we explicitly provide some examples of the estimator (12) by considering standard CFD problems.

4.1. *The elliptic problem.*

First benchmark for the general theory above has been the simple elliptic problem

(13)
$$\begin{cases} L(u) = -\sum_{i,j=1}^{2} \frac{\partial}{\partial x_i} \left(a_{ij} \frac{\partial u}{\partial x_j} \right) + cu = f & \text{in } \Omega, \\ u = 0 & \text{on } \partial\Omega, \end{cases}$$

with $c = c(\boldsymbol{x}) \geq 0$ a.e. in Ω, $f \in L^2(\Omega)$ and $a_{ij} = a_{ij}(\boldsymbol{x})$ given functions. Moreover, the operator L is assumed elliptic, i.e., there exists a constant $\beta > 0$ such that, for any $\boldsymbol{\xi} = (\xi_1, \xi_2)^T \in \mathbb{R}^2$ and for almost every $\boldsymbol{x} \in \Omega$,

$$\sum_{i,j=1}^{2} a_{ij}(\boldsymbol{x}) \, \xi_i \xi_j \geq \beta |\boldsymbol{\xi}|^2,$$

$|\cdot|$ denoting the standard Euclidean norm in $\mathbb{R}^2$. By introducing a continuous piecewise linear finite element approximation, we get the discretization corresponding to (8), where the bilinear and linear forms $a : V \times V \to \mathbb{R}$ and $F : V \to \mathbb{R}$, with $V = H_0^1(\Omega)$, are given by

$$a(u, v) = \int_{\Omega} \left[\sum_{i,j=1}^{2} a_{ij} \frac{\partial u}{\partial x_j} \frac{\partial v}{\partial x_i} + cuv \right] d\boldsymbol{x} \quad \text{and} \quad F(v) = \int_{\Omega} fv \, d\boldsymbol{x},$$

respectively. The procedure detailed above for the derivation of a goal-oriented a posteriori error estimator can be applied to (13) (see [18]). With this aim, let us define the residual of the discrete solution u_h on the triangle K

$$r_K(u_h) = \left[f + \sum_{i,j=1}^{2} \frac{\partial}{\partial x_i} \left(a_{ij} \frac{\partial u_h}{\partial x_j} \right) - cu_h \right] \Big|_K$$

together with the element boundary residual

$$j_e^{\text{Ellip}} = \begin{cases} [\partial_{n_L} u_h]_e & \text{if } e \in \mathcal{E}_h^{\text{int}}, \\ 0 & \text{if } e \in \partial\Omega, \end{cases}$$

where $\mathcal{E}_h^{\text{int}}$ denotes the set of the internal edges of the skeleton $\mathcal{E}_h$ of the triangulation $\mathcal{T}_h$ and $[\partial_{n_L} u_h]_e$ is the jump across the edge $e \in \mathcal{E}_h^{\text{int}}$ of the co-normal derivative of u_h

$$\partial_{n_L} u_h = \sum_{i,j=1}^{2} a_{ij} \frac{\partial u_h}{\partial x_j} n_i,$$

$\boldsymbol{n} = (n_1, n_2)^T$ being the unit outward normal vector. Then we have derived an a posteriori error estimate with the same structure as (12) by assuming either

an H^2- or an H^1-regularity for the dual solution z. In both cases, the element residual $\varrho_K(u_h)$ associated with the primal problem is given by

$$(14) \qquad \varrho_K(u_h) = \|r_K(u_h)\|_{L^2(K)} + \frac{1}{2\lambda_{2,K}^{1/2}}\|j_e^{\text{Ellip}}\|_{L^2(\partial K)},$$

while the element weight $\omega_K(z)$ is defined, for $z \in H^2(\Omega)$, by

$$(15) \qquad \omega_K(z) = \frac{(\lambda_{1,K}^2 + \lambda_{2,K}^2)^{1/2}}{\lambda_{2,K}} \left[\sum_{i,j=1}^{2} \lambda_{i,K}^2 \lambda_{j,K}^2 L_K^{i,j}(z) \right]^{1/2},$$

or, if $z \in H^1(\Omega)$, we have

$$\omega_K(z) = \left[\sum_{i=1}^{2} \lambda_{i,K}^2 \left(\boldsymbol{r}_{i,K}^T G_K(z) \, \boldsymbol{r}_{i,K} \right) \right]^{1/2}.$$

Notice that all the anisotropic information $\lambda_{i,K}$ and $\boldsymbol{r}_{i,K}$ is contained in the weights $\omega_K(z)$. Moreover, it is evident that for $z \in H^2(\Omega)$ the function z_h in (11) is chosen as the Lagrange finite element interpolant of z, while if z is only an $H^1(\Omega)$-function, z_h coincides with the Clément interpolant of z. Finally, we remark that the constant C in (12) depends only on the reference triangle $\widehat{K}$ in the case $z \in H^2(\Omega)$, while $C = C(M, \widehat{C})$ if $z \in H^1(\Omega)$.

4.2. *The advection-diffusion-reaction problem.*

Let us address the standard scalar advection-diffusion-reaction problem with mixed boundary conditions

$$(16) \qquad \begin{cases} L(u) = -\mu\Delta u + \boldsymbol{a} \cdot \nabla u + \alpha u = f & \text{in } \Omega, \\ u = 0 & \text{on } \Gamma_D, \\ \mu\dfrac{\partial u}{\partial n} = g & \text{on } \Gamma_N, \end{cases}$$

where Γ_D and Γ_N are measurable non overlapping partitions of the boundary $\partial\Omega$ of Ω with $\Gamma_D \neq \emptyset$ and such that $\partial\Omega = \overline{\Gamma}_D \cup \overline{\Gamma}_N$; the source $f \in L^2(\Omega)$, the diffusivity $\mu \in \mathbb{R}^+$, the advective field $\boldsymbol{a} \in [W^{1,\infty}(\Omega)]^2$, with $\nabla\cdot\boldsymbol{a} = 0$, the reaction coefficient $\alpha \in L^\infty(\Omega)$ with $\alpha \geqslant 0$ a.e. in Ω, and $g \in L^2(\Gamma_N)$ are given data, while $\partial u/\partial n = \nabla u \cdot \boldsymbol{n}$ is the normal derivative of u, $\boldsymbol{n}$ still denoting the unit outward normal to $\partial\Omega$.

From an anisotropic viewpoint, the most interesting problems are the advection-reaction dominated ones. This justifies the use of a stabilized scheme to discretize (16). Thus, the discrete form (8) reads as follows: find $u_h \in V_h \subset V$, with $V = H^1_{\Gamma_D}(\Omega)$, such that

$$a_\tau(u_h, v_h) = F_\tau(v_h) \quad \text{for any} \quad v_h \in V_h,$$

where the subscript τ refers to stabilized bilinear and linear forms. As we limit our analysis to the case of affine linear finite elements, all the standard stabilized techniques, such as GLS, SUPG [9, 29] and the method proposed by Douglas and Wang in [14], do coincide with each other. For instance, by choosing a streamline-diffusion scheme (see [15]), the stabilized forms $a_\tau\colon V \times V \to \mathbb{R}$ and $F_\tau\colon V \to \mathbb{R}$ are defined, for smooth enough functions u and v, as

$$a_\tau(u, v) = \int_\Omega \mu \nabla u \cdot \nabla v \, d\boldsymbol{x} + \int_\Omega (\boldsymbol{a} \cdot \nabla u + \alpha u) \, v \, d\boldsymbol{x}$$

(17)
$$+ \sum_{K \in \mathscr{C}_h} \int_K \tau_K(-\mu \Delta u + \boldsymbol{a} \cdot \nabla u + \alpha u)(\boldsymbol{a} \cdot \nabla v) \, d\boldsymbol{x},$$

$$F_\tau(v) = \int_\Omega f v \, d\boldsymbol{x} + \int_{\Gamma_N} g v \, ds + \sum_{K \in \mathscr{C}_h} \int_K \tau_K f(\boldsymbol{a} \cdot \nabla v) \, d\boldsymbol{x} \,.$$

The coefficients τ_K are elementwise stabilizing parameters for which several proposals are available in the literature (see, e.g., [4, 7, 8, 32]).

By mimicking the procedure of Sect. 4, we get also for problem (16) an anisotropic a posteriori error estimator of the form (12) (see [19] for the details). Let us define the element interior and boundary residuals given by $r_K(u_h) = (f + \mu \Delta u_h - \boldsymbol{a} \cdot \nabla u_h - \alpha u_h)|_K$ and

(18)
$$j_e^{\mathrm{Adr}} = \begin{cases} 0 & \text{if } e \in \Gamma_D, \\[2mm] -2\left(\mu \dfrac{\partial u_h}{\partial n_K} - g\right) & \text{if } e \in \Gamma_N, \\[2mm] -\mu \left[\dfrac{\partial u_h}{\partial n_K}\right]_e & \text{if } e \in \mathscr{E}_h^{\mathrm{int}}, \end{cases}$$

respectively. Here $\partial u_h/\partial n_K = \nabla u_h \cdot \boldsymbol{n}_K$ is the normal derivative of u_h, $\boldsymbol{n}_K$ is the unit outward normal to ∂K, $\mathscr{E}_h^{\mathrm{int}}$ still denotes the set of the internal edges of the triangulation $\mathscr{C}_h$, while $[\partial u_h/\partial n_K]_e$ stands for the jump of the normal derivative of u_h over the edge $e \subset \partial K$. Then the residual $\varrho_K(u_h)$ is given by

(19) $$\varrho_K(u_h) = \|r_K(u_h)\|_{L^2(K)} \left(1 + \frac{\tau_K}{\lambda_{2,K}} \|\boldsymbol{a}\|_{L^\infty(K)}\right) + \frac{1}{2\lambda_{2,K}^{1/2}} \|j_e^{\mathrm{Adr}}\|_{L^2(\partial K)}.$$

By assuming an H^1-regularity for the dual solution z, we identify z_h in (11) with the Clément interpolant of z. This yields for the weights $\omega_K(z)$ the expression

$$\omega_K(z) = \left[\sum_{i=1}^2 \lambda_{i,K}^2 \left(\boldsymbol{r}_{i,K}^T G_K(z) \, \boldsymbol{r}_{i,K}\right)\right]^{1/2}.$$

In such a case the constant C in (12) depends on the constants M and $\widehat{C}$ defined in (4).

The a posteriori analysis above has been applied both to academic test cases, such as the one shown in Sect. **5**, and to a more realistic problem in haemodynamics [20].

REMARK 4.1. – *By letting $\boldsymbol{a} = 0$ in (19), as a particular case of the analysis above we recover the a posteriori result for the diffusion-reaction problem (13) provided with mixed boundary conditions.*

REMARK 4.2. – *When the discretization of the primal problem involves a stabilization procedure, it is not so unusual to stabilize also the weak form (10) of the dual problem. Even if the stabilization is usually applied to the discrete formulation only, it has been verified an improvement of the convergence rate (superconvergence) of the error estimator in the presence of a stabilized weak form of the dual problem [7].*

4.3. *The Stokes problem.*

We consider the standard Stokes problem: seek the velocity $\boldsymbol{u}$ and the pressure p of an incompressible fluid, subject to mixed boundary conditions, such that

$$
(20) \quad
\begin{cases}
-\mu \Delta \boldsymbol{u} + \nabla p = \boldsymbol{f} & \text{in } \Omega, \\
\nabla \cdot \boldsymbol{u} = 0 & \text{in } \Omega, \\
\mu(\nabla \boldsymbol{u})\,\boldsymbol{n} - p\boldsymbol{n} = \boldsymbol{g} & \text{on } \Gamma_N, \\
\boldsymbol{u} = \boldsymbol{0} & \text{on } \Gamma_D,
\end{cases}
$$

where Γ_D, Γ_N and $\boldsymbol{n}$ are defined as in Sect. 4.2; the source term $\boldsymbol{f} \in [L^2(\Omega)]^2$, the viscosity $\mu \in \mathbb{R}^+$ and $\boldsymbol{g} \in [L^2(\Gamma_N)]^2$ are given data. Notice that the differential operator $L(u)$ in (6) is now replaced by the operator $L(\boldsymbol{u}, p)$ represented by the left-hand sides of $(20)_1$-$(20)_2$. Moreover, the weak space V in (7) is replaced by the tensor product space $W \times Q$, with $W = [H^1_{\Gamma_D}(\Omega)]^2$ and $Q = L^2(\Omega)$. We recall that, in the case $\Gamma_N = \emptyset$, $W = [H^1_0(\Omega)]^2$ and the space Q coincides with $L^2_0(\Omega) = \{v \in L^2(\Omega) \text{ s.t. } \int_\Omega v\,d\boldsymbol{x} = 0\}$.

Since we discretize both the velocity $\boldsymbol{u}$ and the pressure p in (20) by continuous piecewise linear finite elements, we have to adopt a stabilized method in order to guarantee the inf-sup condition, i.e., the well-posedness of the Stokes problem [9, 14, 21, 28]. As in the case of the advection-diffusion-reaction problem, the choice of the stabilization scheme is irrelevant as we are using linear finite elements. For instance, the Galerkin Least-Squares method [22, 28] yields the stabilized discrete form of (20): find $(\boldsymbol{u}_h, p_h)$ in $W_h \times Q_h \subset W \times Q$

such that

$$a_\tau((\boldsymbol{u}_h, p_h),(\boldsymbol{v}_h, q_h)) = F_\tau(\boldsymbol{v}_h, q_h) \quad \text{for any} \quad (\boldsymbol{v}_h, q_h) \in W_h \times Q_h,$$

where the stabilized forms $a_\tau : [W \times Q]^2 \to \mathbb{R}$ and $F_\tau : W \times Q \to \mathbb{R}$ are given by

$$a_\tau((\boldsymbol{u}, p),(\boldsymbol{v}, q)) = \int_\Omega \mu \nabla \boldsymbol{u} : \nabla \boldsymbol{v}\, d\boldsymbol{x} - \int_\Omega p \nabla \cdot \boldsymbol{v}\, d\boldsymbol{x} - \int_\Omega q \nabla \cdot \boldsymbol{u}\, d\boldsymbol{x}$$

(21)
$$- \sum_{K \in \mathcal{C}_h} \tau_K \int_K \nabla p \cdot \nabla q\, d\boldsymbol{x}$$

$$F_\tau(\boldsymbol{v}, q) = \int_\Omega \boldsymbol{f} \cdot \boldsymbol{v}\, d\boldsymbol{x} + \int_{\Gamma_N} \boldsymbol{g} \cdot \boldsymbol{v}\, ds - \sum_{K \in \mathcal{C}_h} \tau_K \int_K \boldsymbol{f} \cdot \nabla q\, d\boldsymbol{x}\,.$$

Several proposals are available in the literature to choose the elementwise stabilizing parameters τ_K in (21) [22, 32, 33].

As now problem (20) has two unknowns, we are in a position to control two continuous linear functionals, the first one $J_1(\cdot)$ associated with the discretization error $\boldsymbol{e}_u = \boldsymbol{u} - \boldsymbol{u}_h$ of the velocity and the second one $J_2(\cdot)$ related to the discretization error $e_p = p - p_h$ of the pressure. Likewise, we can define either the element interior and boundary residuals associated with the momentum equation $(20)_1$, $\boldsymbol{r}_K^1(\boldsymbol{u}_h, p_h) = (\boldsymbol{f} + \mu \Delta \boldsymbol{u}_h - \nabla p_h)|_K$ and

$$\boldsymbol{j}_e^{\text{Stokes}} = \begin{cases} \boldsymbol{0} & \text{if } e \in \Gamma_D, \\ 2(\boldsymbol{g} - (\mu(\nabla \boldsymbol{u}_h \boldsymbol{n}_K) - p_h \boldsymbol{n}_K)) & \text{if } e \in \Gamma_N, \\ -[(\mu(\nabla \boldsymbol{u}_h \boldsymbol{n}_K) - p_h \boldsymbol{n}_K)]_e & \text{if } e \in \mathcal{E}_h^{\text{int}}, \end{cases}$$

respectively, or the interior residual $r_K^2(\boldsymbol{u}_h) = (\nabla \cdot \boldsymbol{u}_h)|_K$ related to the continuity equation $(20)_2$. Here $\mu(\nabla \boldsymbol{u}_h \boldsymbol{n}_K) - p_h \boldsymbol{n}_K$ is the normal component of the Cauchy stresses, the quantities $\boldsymbol{n}_K, \mathcal{E}_h^{int}$ and $[\cdot]_e$ being defined as in Sect. 4.2.

The generic a posteriori analysis provided above can be extended to the case of systems of partial differential equations. In the case of problem (20), the a posteriori estimate (12) is replaced by the new one

(22) $\quad |J_1(\boldsymbol{e}_u) + J_2(e_p)| \leqslant C \sum_{K \in \mathcal{C}_h} (\varrho_K^1(\boldsymbol{u}_h, p_h)\, \omega_K^1(\boldsymbol{w}) + \varrho_K^2(\boldsymbol{u}_h, p_h)\, \omega_K^2(r)),$

with $C = C(M, \widehat{C}, \widehat{K})$ and $(\boldsymbol{w}, r)$ the dual velocity-pressure pair, while

$$\varrho_K^1(\boldsymbol{u}_h, p_h) = \|\boldsymbol{r}_K^1(\boldsymbol{u}_h, p_h)\|_{L^2(K)} + \frac{1}{2}\left(\frac{\lambda_{1,K}^2 + \lambda_{2,K}^2}{\lambda_{2,K}^3}\right)^{1/2}\|\boldsymbol{j}_e^{\mathrm{Stokes}}\|_{L^2(\partial K)},$$

$$\varrho_K^2(\boldsymbol{u}_h, p_h) = \|r_K^2(\boldsymbol{u}_h)\|_{L^2(K)} + \frac{\tau_K}{\lambda_{2,K}}\|\boldsymbol{r}_K^1(\boldsymbol{u}_h, p_h)\|_{L^2(K)},$$

$$\omega_K^1(\boldsymbol{w}) = \left[\sum_{i,j=1}^{2}\lambda_{i,K}^2\lambda_{j,K}^2 L_K^{i,j}(\boldsymbol{w})\right]^{1/2},$$

$$\omega_K^2(r) = \left[\sum_{i=1}^{2}\lambda_{i,K}^2(\boldsymbol{r}_{i,K}^T G_K(r)\,\boldsymbol{r}_{i,K})\right]^{1/2},$$

where the quantities $L_K^{i,j}(\boldsymbol{w})$ are the straightforward extension to vector-valued functions of the terms (2) (see [19, 32] for the details). The test-functions pair $(\boldsymbol{w}_h, r_h)$ corresponding to z_h in (11), has been chosen as $(\Pi_h(\boldsymbol{w}), I_h(r))$ because of the regularity characterizing the velocity and the pressure of the Stokes problem (20). Finally, we point out that (22) consists of the contributions associated with the error propagation due to both the dual velocity and the dual pressure.

5. – Numerical results.

A typical numerical adaptive process for the approximation of a given problem consists of an iterative procedure based on the concept of metric. Starting from an a posteriori error estimator, a second-order tensor field, collecting the information about the mesh spacing and orientation, is defined on the actual mesh and employed for the generation of the new mesh.

In the first part of this section we provide some further detail on the adaptive algorithm used for the construction of an «optimal» mesh, i.e., the mesh for which we have maximum accuracy for a given number of degrees of freedom. Then we assess the soundness of the adopted procedure on some academic test cases, by referring to [17, 18, 19, 20, 32] for a larger range of numerical examples.

5.1. *The adaptive procedure.*

The anisotropic information provided by the error estimators in Sects. 4.1, 4.2 and 4.3 can be employed within a mesh adaption procedure in a *predictive fashion*. A standard technique consists of endowing the domain Ω with a *metric* updated via an iterative process by employing the data stemming from the actual mesh. A possible metric for the domain Ω is identified by a symmetric positive definite tensor field $\widetilde{M}$ such that $\widetilde{M} = \widetilde{R}\widetilde{\Lambda}^{-2}\widetilde{R}^{\mathrm{T}}$, where $\widetilde{\Lambda} = $

diag $(\tilde{\lambda}_1, \tilde{\lambda}_2)$ and $\tilde{R}^{\mathrm{T}} = (\tilde{\boldsymbol{r}}_1, \tilde{\boldsymbol{r}}_2)$ are a positive diagonal and an orthogonal matrix, respectively. The matrix $\tilde{M}$ should be chosen in order that the newly generated mesh satisfies (as far as possible) an *optimality criterion*, requiring that all the edges of the new mesh be of unit length according to the metric induced by $\tilde{M}$. Thus, the metric $\tilde{M}$ is identified when $\tilde{\lambda}_1, \tilde{\lambda}_2, \tilde{\boldsymbol{r}}_1, \tilde{\boldsymbol{r}}_2$ are determined. For this purpose, we approximate these quantities by piecewise constant functions over the triangulation $\mathcal{C}_h$, that is $\tilde{\boldsymbol{r}}_i |_K = \tilde{\boldsymbol{r}}_{i,K}$ and $\tilde{\lambda}_i |_K = \tilde{\lambda}_{i,K}$, with $i = 1, 2$.

Relation (12) defines a local estimator η_K, such that

$$|J(e_h)| \leqslant C \sum_{K \in \mathcal{C}_h} \eta_K,$$

with $\eta_K = \varrho_K(u_h) \, \omega_K(z)$. After a suitable scaling of η_K, we resort to two classical requirements for a mesh adaption procedure: i) *equidistributing* the error, and ii) *maximizing* the area of the triangles, i.e. minimizing the degrees of freedom of the new mesh. More precisely, since we can only act on the local estimators, we impose on the one hand that $\eta_K = \tau$, for any $K \in \mathcal{C}_h$, where τ is a given tolerance, and on the other hand that $|K|$ be as large as possible. This amounts to solving a minimization problem involving the L_K's and/or the G_K's terms, for s_K and $\boldsymbol{r}_{1,K}$ (see [19] for all the details). Finally, by denoting with $\tilde{s}_K = \tilde{\lambda}_{1,K}/\tilde{\lambda}_{2,K}$ and $\tilde{\boldsymbol{r}}_{1,K}$ the solution of such a minimization problem, we use requirement i) to obtain separately the two values $\tilde{\lambda}_{1,K}$ and $\tilde{\lambda}_{2,K}$. The metric $\tilde{M}$ is thus identified.

5.2. *Numerical assessment.*

In the subsections below we test the effectiveness of the adaptive procedure described above on three test cases, one for each of the differential problems in Sects. 4.1, 4.2 and 4.3. The software used for the mesh generation is BAMG [27].

We highlight that here we are not interested in discussing how the solution z of the dual problem is actually computed. In other words, we are not concerned with the discretization issue of the dual problem: we just assume that we have some accurate enough approximation of z to compute the L_K's and the G_K's quantities (see also [2]).

The elliptic case.

Let us apply the a posteriori analysis of Sect. 4.1 to an elliptic toy problem, namely the Poisson equation

$$(23) \qquad\qquad -\Delta u = f \quad \text{in} \quad \Omega = (0, 1)^2,$$

provided with homogeneous Dirichlet boundary conditions. The forcing term f is chosen in such a way that the exact solution u of (23) is

$$u(x_1, x_2) = 4x_2(1 - x_2)[1 - e^{-ax_1} - (1 - e^{-a}) x_1],$$

with $\alpha = 100$. The function u exhibits an exponential layer along the boundary $x = 0$ with an initial steepness of α. The presence of the boundary layer justifies the employment of an anisotropic mesh adaption technique.

As $u \in H^2(\Omega)$, we have applied the adaption procedure of Sect. 5.1 to the error estimator (12) identified by the residual $\varrho_K(u_h)$ in (14) and by the weights $\omega_K(z)$ defined in (15). As goal quantity to be controlled we choose the flux of the solution u across the boundary edge $x = 0$, i.e.

$$(24) \qquad J(\varphi) = \int_0^1 \frac{\partial \varphi}{\partial x}(0, y)\, dy \,.$$

Notice that, to apply the analysis of Sect. 4, we need to regularize the functional J as it is not linear on $H^1(\Omega)$. With this aim, we replace (24) with the regularized one

$$J^*(\varphi) = \int_0^1 \frac{\varphi(\varepsilon, y) - \varphi(0, y)}{\varepsilon}\, dy \quad \text{for any} \quad \varphi \in H^1(\Omega) \,,$$

ε being a small positive constant, here taken equal to 0.04. By starting the adaptive procedure of Sect. 5.1 on an initial uniform mesh of about 1000 triangles, we get the anisotropic mesh of Fig. 3 (left) which has approximately 2500 elements. The regions of the computational domain Ω more affecting the evaluation of the goal quantity, are detected by the anisotropic error estimator as the distribution of the mesh triangles highlights. To underline the advantages deriving from an anisotropic mesh adaption, let us consider the isotropic mesh on the right of Fig. 3 obtained simply by choosing $\lambda_{1,K} = \lambda_{2,K}$ and $r_{1,K} \equiv r_{2,K}$ in (15). The two grids have approximately the same number of elements but the functional of the discretization error e_h is given by $|J^*(e_h^{\text{aniso}})| = 7.8 \times 10^{-3}$ in the anisotropic case while, with the isotropic
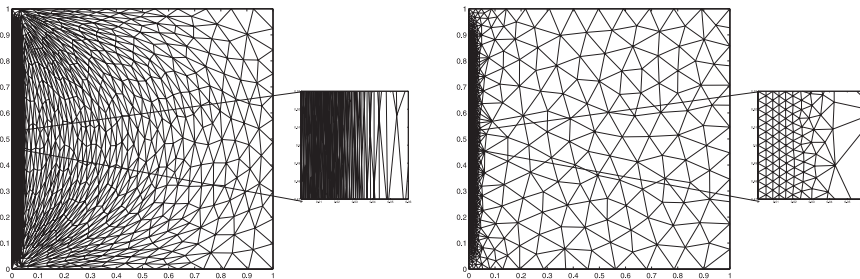
Fig. 3. – An adapted anisotropic mesh (left) compared with the corresponding isotropic one (right) for the Poisson problem (23). Both grids have approximately 2500 elements.

grid, we have $|J^*(e_h^{\text{iso}})| = 30.0 \times 10^{-3}$. A reduction of more than one-third is guaranteed in the anisotropic case.

We finally refer to [18] where other numerical examples for the elliptic case are provided.

The advection-diffusion-reaction case.

A typical instance of problems exhibiting directional features are the advection dominated problems.

Let $\Omega = (0, 1)^2$ be the computational domain. Then we choose $\mu = 10^{-4}$, $\boldsymbol{a} = (2, 1)^T$, $\alpha = 0$ and $f = 0$ in (16). Let us assign Dirichlet conditions on all the boundary $\partial \Omega$: in more detail, we demand $u = 1$ on the left and top sides of Ω and $u = 0$ on the remaining edges. This choice yields a solution u characterized by an internal and a boundary layer of thickness $\mathcal{O}(10^{-2})$ and $\mathcal{O}(10^{-4})$, respectively.

The functional J in (10) is chosen as $J(\varphi) = a_0(\varphi, u)$, for any $\varphi \in V$, where the subscript 0 refers to the non-stabilized bilinear form derived from (17). This choice allows us to control the energy norm of the discretization error, as $J(e_h) = a_0(u - u_h, u) = a_0(u - u_h, u - u_h)$, thanks to the Galerkin orthogonality property (9).

Moving from an initial uniform mesh of about 350 elements, after two steps of the adaptive procedure described in Sect. 5.1, we get the anisotropic mesh shown in Fig. 4 (in the middle).

It is evident that the two layers are sharply captured and their thickness is correctly detected. The orientation and deformation of the mesh elements (longest edges parallel to the boundary layers) thus guarantee a reduction of the number of triangles, that is of the computational cost associated with the approximation of the problem at hand.

The numerical solution computed on the adapted grid and a zoom of the mesh in correspondence of the boundary layer are also provided on the left and on the right of Fig. 4, respectively.

We finally remark that, even if the analysis of Sect. 4.2 has been derived for mixed boundary conditions, it can be easily extended to the case of full
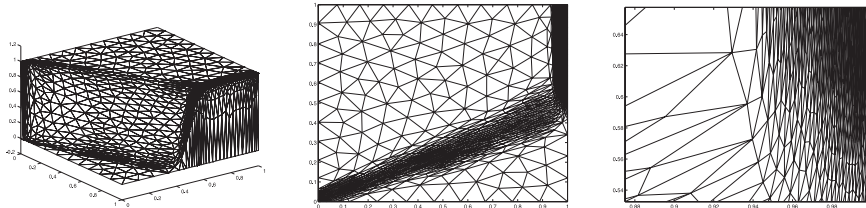
Fig. 4. – Numerical solution (left) computed on the second anisotropic adapted mesh (middle) and a zoom of the boundary layer (right).

Dirichlet boundary conditions, provided that the definitions of the functional space V and of the boundary residual j_e^{Adr} in (18) are properly modified.

The Stokes problem case.

We assess the soundness of the a posteriori estimate (22) on a standard numerical example, the driven cavity flow test case. The motion of a flow inside a plane square domain $\Omega = (0, 1)^2$, with velocity $\boldsymbol{u} = (1, 0)^T$ prescribed on the top boundary, is analyzed. Furthermore, a no-slip boundary condition is imposed on the vertical sides as well as on the bottom horizontal side and μ is chosen equal to 10^{-1}. This choice for the boundary conditions yields a pressure field p characterized by two spikes at the points $(0, 1)$ and $(1, 1)$.

The adaptive procedure of Sect. 5.1 has been extended to the error estimator (22). The presence of the two goal functionals J_1 and J_2 leads to a minimization problem involving both the L_K's and the G_K's terms. In this case, we solve two decoupled subproblems for $\tilde{s}_K$ and $\tilde{r}_{1,K}$, the first one associated with the L_K's terms and the second one with the G_K's terms. Two metrics $\widetilde{M}_1$ and $\widetilde{M}_2$ are thus derived from the two subproblems. The final metric $\widetilde{M}$ is obtained by summing the metrics $\widetilde{M}_1$ and $\widetilde{M}_2$, weighted with the corresponding residuals [24].

As in the previous test cases, we start the adaptive procedure on an initial uniform mesh, of about 1300 elements. The target functionals J_1 and J_2 in (22) are chosen as $J_1(\boldsymbol{v}) = 0$ and $J_2(q) = \int_\Omega 2pq\,d\boldsymbol{x}$. This choice allows us to control the L^2-norm of the pressure through the linearized functional $J_2(q)$.

The pressure fields computed on the initial and on the second adapted grid (6136 triangles) are shown in Fig. 5. The two spikes at the points $(0, 1)$ and
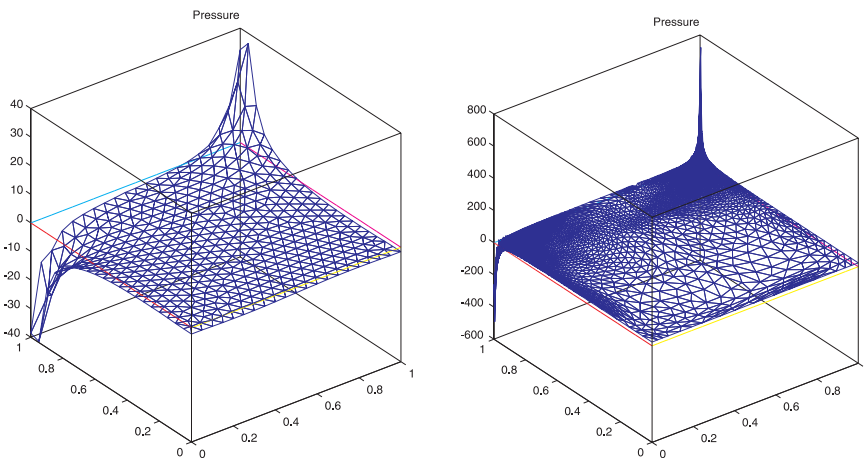
Fig. 5. – Pressure fields computed on the initial uniform mesh and the second anisotropic adapted one.

$(1, 1)$ are not well captured on the initial mesh (see Fig. 5, on the left), while the anisotropic adapted mesh turns out to be better to capture these features (Fig. 5, right, compare the vertical scales of the two plots).

6. – Conclusions.

In this paper we have presented a goal-oriented anisotropic adaption technique combining the good properties of the error functional control theory in [7], with the richness of information provided by the anisotropic framework in [17]. As examples of this general theory we consider the elliptic, advection-diffusion-reaction and the Stokes problems. A numerical validation is also carried out to assess the soundness of the theoretical approach.

REFERENCES

[1] M. AINSWORTH - J. T. ODEN, *A posteriori error estimation in finite element analysis*, John Wiley & Sons, Inc., New-York, 2000.

[2] R. C. ALMEIDA - R. A. FEIJÓO - A. C. GALEÃO - C. PADRA - R. S. SILVA, *Adaptive finite element computational fluid dynamics using an anisotropic error estimator*, Comput. Methods Appl. Mech. Engrg., **182** (2000), 379-400.

[3] T. APEL, *Anisotropic finite elements: local estimates and applications*, Book Series: Advances in Numerical Mathematics, Teubner, Stuttgart, 1999.

[4] T. APEL - G. LUBE, *Anisotropic mesh refinement in stabilized Galerkin methods*, Numer. Math., **74** (1996), 261-282.

[5] I. BABUŠKA - W. RHEINBOLDT, *A posteriori error estimates for the finite element method*, Int. J. Numer. Methods Eng., **12** (1978), 1597-1615.

[6] R. E. BANK - A. WEISER, *Some a posteriori error estimators for elliptic partial differential equations*, Math. Comp., **44**, no. 170 (1985), 283-301.

[7] R. BECKER - R. RANNACHER, *An optimal control approach to a posteriori error estimation in finite element methods*, Acta Numerica, **10** (2001), 1-102.

[8] F. BREZZI - A. RUSSO, *Choosing bubbles for advection-diffusion problems*, Math. Models Methods Appl. Sci., **4** (1994), 571-587.

[9] A. N. BROOKS - T. J. R. HUGHES, *Streamline upwind / Petrov-Galerkin formulations for convective dominated flows with particular emphasis on the incompressible Navier-Stokes equations*, Comput. Methods Appl. Mech. Engrg., **32** (1982), 199-259.

[10] PH. CIARLET, *The finite element method for elliptic problems*, North-Holland Publishing Company, Amsterdam, 1978.

[11] Ph. Clément, *Approximation by finite element functions using local regularization*, RAIRO Anal. Numér., **2** (1975), 77-84.

[12] D. L. Darmofal - D. A. Venditti, *Anisotropic grid adaptation for functional outputs: application to two-dimensional viscous flows*, J. Comput. Phys., **187** (2003) 22-46.

[13] E. F. D'Azevedo - R. B. Simpson, *On optimal triangular meshes for minimizing the gradient error*, Numer. Math., **59** (1991), 321-348.

[14] J. Douglas - J. Wang, *An absolutely stabilized finite element method for the Stokes problem*, Math. Comp., **52** (1989), 495-508.

[15] K. Eriksson - C. Johnson, *Adaptive streamline diffusion finite element methods for stationary convection-diffusion problems*, Math. Comp., **60** (1993), 167-188.

[16] K. Eriksson - D. Estep - P. Hansbo - C. Johnson, *Introduction to adaptive methods for differential equations*, Acta Numerica, (1995), 105-158.

[17] L. Formaggia - S. Perotto, *New anisotropic a priori error estimates*, Numer. Math., **89** (2001), 641-667.

[18] L. Formaggia - S. Perotto, *Anisotropic error estimates for elliptic problems*, Numer. Math., **94** (2003), 67-92.

[19] L. Formaggia - S. Micheletti - S. Perotto, *Anisotropic mesh adaptation in Computational Fluid Dynamics: application to the advection-diffusion-reaction and the Stokes problems*, to appear in Appl. Num. Math. (2004).

[20] L. Formaggia - S. Perotto - P. Zunino, *An anisotropic a-posteriori error estimate for a convection-diffusion problem*, Comput. Visual. Sci., **4** (2001), 99-104.

[21] L. P. Franca - T. J. R. Hughes, *Convergence analyses of Galerkin least-squares methods for symmetric advective-diffusive forms of the Stokes and incompressible Navier-Stokes equations*, Comput. Methods Appl. Mech. Engrg., **105** (1993), 285-298.

[22] L. Franca - R. Stenberg, *Error analysis of some GLS methods for elasticity equations*, SIAM J. Numer. Anal., **28** (1991), 1680-1697.

[23] F. Courty - D. Leservoisier - P. L. George - A. Dervieux, *Continuous metrics and mesh optimization*, submitted for the publication in Appl. Numer. Math., (2003).

[24] P. L. George - H. Borouchaki, *Delaunay triangulation and meshing-application to finite element*, Editions Hermes, Paris, 1998.

[25] M. B. Giles - E. Süli, *Adjoint methods for PDEs: a posteriori error analysis and postprocessing by duality*, Acta Numerica, **11** (2002), 145-236.

[26] W. G. Habashi - M. Fortin - J. Dompierre - M. G. Vallet - Y. Bourgault, *Anisotropic mesh adaptation: a step towards a mesh-independent and user-independent CFD*, in Barriers and Challenges in Computational Fluid Dynamics, Kluwer Acad. Publ., 1998, 99-117.

[27] F. Hecht, *BAMG: bidimensional anisotropic mesh generator*, (1998). http://www-rocq.inria.fr/gamma/cdrom/www/bamg/eng.htm

[28] T. J. R. Hughes - L. Franca - M. Balestra, *A new finite element formulation for computational fluid dynamics. V. Circumventing the Babuška-Brezzi condition: a stable Petrov-Galerkin formulation of the Stokes problem accommodating equal-order interpolations*, Comput. Methods Appl. Mech. Engrg., **59** (1986), 85-99.

[29] T. J. R. Hughes - L. P. Franca - G. M. Hulbert, *A new finite element formulation for computational fluid dynamics: VIII. the Galerkin/least-squares method for advective-diffusive equations*, Comput. Methods Appl. Mech. Engrg., **73** (1989), 173-189.

[30] G. Kunert, *A posteriori error estimation for anisotropic tetrahedral and triangular finite element meshes*, Ph.D. thesis, Fakultät für Mathematik der Technischen Universität Chemnitz, Chemnitz, 1999.

[31] J. L. LIONS - E. MAGENES, *Non-homogeneous boundary value problem and application*, Volume I. Springer-Verlag, Berlin, 1972.

[32] S. MICHELETTI - S. PEROTTO - M. PICASSO, *Stabilized finite elements on anisotropic meshes: a priori error estimates for the advection-diffusion and Stokes problems*, SIAM J. Numer. Anal., **41**, no. 3 (2003), 1131-1162.

[33] S. MITTAL, *On the performance of high aspect ratio elements for incompressible flows*, Comput. Methods Appl. Mech. Engrg., **188** (2000), 269-287.

[34] J. T. ODEN - S. PRUDHOMME, *Goal-oriented error estimation and adaptivity for the finite element method*, Computers Math. Applic., **41**, no. 5-6 (2001), 735-756.

[35] M. PICASSO, *An anisotropic error indicator based on Zienkiewicz-Zhu error estimator: application to elliptic and parabolic problems*, SIAM J. Sci. Comput., **24**, no. 4 (2003), 1328-1355.

[36] L. R. SCOTT - S. ZHANG, *Finite element interpolation of non-smooth functions satisfying boundary conditions*, Math. Comp., **54** (1990), 483-493.

[37] K. G. SIEBERT, *An a posteriori error estimator for anisotropic refinement*, Numer. Math., **73** (1996), 373-398.

[38] R. VERFÜRTH, *A review of a posteriori error estimation and adaptive mesh-refinement techniques*, B. G. Teubner, Stuttgart, 1996.

[39] O. C. ZIENKIEWICZ - J. Z. ZHU, *A simple error estimator and adaptive procedure for practical engineering analysis*, Int. J. Numer. Methods Eng., **24** (1987), 337-357.

[40] O. C. ZIENKIEWICZ - J. Z. ZHU, *The superconvergent patch recovery and a posteriori error estimates, Part 1: the recovery technique*, Int. J. Numer. Methods Eng., **33** (1992), 1331-1364.

[41] O. C. ZIENKIEWICZ - J. Z. ZHU, *The superconvergent patch recovery and a posteriori error estimates, Part 2: error estimates and adaptivity*, Int. J. Numer. Methods Eng., **33** (1992), 1365-1382.

Simona Perotto: MOX-Department of Mathematics «F. Brioschi»,
Politecnico of Milano, Via Bonardi 9, 20133 Milano, Italy
simona.perotto@mate.polimi.it